Microchimica Acta
https://doi.org/10.1007/s00604-017-2631-3

ORIGINAL PAPER

3D nitrogen-doped graphite foam@Prussian blue: an electrochemical sensing platform for highly sensitive determination of H_2O_2 and glucose

Yu Zhang[1] · Bintong Huang[1] · Feng Yu[2] · Qunhui Yuan[3] · Meng Gu[4] · Junyi Ji[5] · Yang Zhang[6,7] · Yingchun Li[7]

Received: 12 September 2017 / Accepted: 22 December 2017

Abstract

A platform is described for voltammetric sensing of hydrogen peroxide (H_2O_2). It is based on the use of nitrogen-doped graphite foam modified with Prussian Blue particles (PB/NGF). Graphite foam was synthesized by chemical vapor deposition, and doping with nitrogen was realized via dielectric barrier plasma discharge. PB particles were grown on the NGF through electrodeposition. SEM images of NGF verified the porous and interconnected structure of graphite foam, and XPS and Raman spectroscopy verified the successful doping with N. The performance of the PB/NGF electrode was characterized by CV and EIS which showed it to possess outstanding properties in terms of sensing H_2O_2. H_2O_2 was quantified in a range of 0.004 to 1.6 mM with a detection limit of 2.4 μM. The PB/NGF electrode also is shown to be a viable substrate for loading glucose oxidase (GOx). The GOx-functionalized electrode responds to glucose over the 0.2 to 20 mM concentration range at a potential of −50 mV (vs. Ag/AgCl), with a sensitivity of 27.48 mA M^{-1} cm^{-2} and a 0.1 M detection limit (at an S/N ratio of 3). The glucose sensor is selective, stable, and reproducible. The biosensor was successfully applied to the determination of glucose in spiked human serum samples, and this confirmed it practicability.

Keywords Biosensor · Nitrogen doped graphene foam · Glucose oxidase · Hydrogen peroxide · Dielectric barrier discharge plasma · Prussian blue · Amperometry · Scanning electron microscopy · X-ray photoelectron spectroscopy · Raman spectra

Introduction

Electrochemical sensors feature fast response, high sensitivity and low detection costs [1, 2]. However, sensors have inherent shortcoming that they lack separation ability in complex samples. To tackle poor selectivity of sensors and improve detection accuracy, proper modification of sensing platform is necessary. Bioreceptors like enzyme [3], antibody [4] and nuclear acid [5] are some important agents as target recognizer for sensor decoration. Biological activity, catalytic efficiency and adequate operation lifespan of the loaded bio-receptors are very critical in sensor system,

Electronic supplementary material The online version of this article (https://doi.org/10.1007/s00604-017-2631-3) contains supplementary material, which is available to authorized users.

✉ Yang Zhang
zhangyang07@hit.edu.cn

✉ Yingchun Li
liyingchun@hit.edu.cn

[1] Key Laboratory of Xinjiang Plant Resources and Utilization, Ministry of Education, School of Pharmacy, Shihezi University, Shihezi 832000, China

[2] Key Laboratory for Green Processing of Chemical Engineering of Xinjiang Bingtuan, School of Chemistry and Chemical Engineering, Shihezi University, Shihezi 832003, China

[3] School of Materials Science and Engineering, Harbin Institute of Technology, Shenzhen 518055, China

[4] Department of Materials Science and Engineering, Southern University of Science and Technology, Shenzhen 518055, China

[5] Collage of Chemical Engineering, Sichuan University, Chengdu 610000, China

[6] Shenzhen Key Laboratory of Organic Pollution Prevention and Control, Harbin Institute of Technology (Shenzhen), Shenzhen, Guangdong 518055, China

[7] College of Science, Harbin Institute of Technology, Shenzhen 518055, China

Published online: 08 January 2018

where decent biocompatibility and immobilization capability of sensor interface are required. Besides, large surface area, lots of functional groups and good electron transport capacity are also admirable merits for loading platform.

Graphite foam (GF) is a kind of three-dimensional (3D) graphene-based material with unique structure and remarkable conductivity [6, 7]. Compared to other carbon materials [8], GF has the following extraordinary properties: The 3D porous skeleton is more accessible for transport of electrolyte and analyte; its good mechanical strength allows its use as a free-standing electrode; interconnected conductive structure with multiple electronic channels is helpful for fast and sensitive detection; high specific surface area coming from lots of folds on GF surface is beneficial for loading large numbers of biomacromolecules. Previously, our group fabricated a GF-based supportless electrochemical sensor, which was modified with so-called artificial Ab-molecularly imprinted polymer and realized ultra-sensitive and selective detection of dopamine [9].

3D GF is short of defects and of poor hydrophilicity [10]. This makes it hardly amenable to further modification like enzyme immobilization. A number of studies have demonstrated that existence of heteroatoms in carbon skeleton allows for significant enhancement of electrochemical characteristics of carbon materials [11]. Nitrogen (N), for instance, is one of the most commonly doped heteroatoms [12], and the material shows n-type or metallic behavior, which is expected to endow better electron mobility. Besides, it has been reported that N-doped carbon nanotubes are more biocompatible and hydrophilic in comparison with non-doped ones due to the potential hydrogen bonds induced by nitrogen [13]. All above merits make N doping an appropriate strategy for graphene functionalization.

Oxidase serves as terminal receptor for more than 90% enzyme-based sensors [14]. Hydrogen peroxide (H_2O_2) is a side product in many enzyme-catalyzed reactions and its detection is one of the most important ways for biosensing [15]. Prussian blue (PB), well known as "artificial peroxidase", has been extensively used as an effective low-potential electron transfer mediator for constructing oxidase-based biosensors, due to its excellent electrocatalytic ability toward H_2O_2 reduction reaction [16, 17]. Therefore, combining good electrochemical performance of N-doped GF (NGF) with good electrocatalysis of PB particles, the hybrid sensor (PB/NGF) can be a promising platform for immobilization of oxidases and detection of corresponding substrates.

In present study, we developed a novel electrode platform for enzyme loading by coupling nitrogen doped GF with PB particles. Firstly, GF was prepared via chemical vapor deposition method with nickel foam template. After removal of nickel, nitrogen doping of GF was realized through dielectric barrier discharge (DBD) plasma. PB particles were further electrodeposited on NGF. Practicability of PB/NGF as an enzyme carrier was demonstrated by loading the electrode with a model enzyme-glucose oxidase (GOx). The biosensor was then successfully applied to detect glucose in human serum.

Experimental

Reagents

Glucose oxidase (GOx, 100 U/mg) was bought from Sigma-Aldrich (Shanghai, China; www.sigmaaldrich.com). Bovine serum albumin (BSA > 98%) was purchased from Biosharp (Hefei, China; www.biosharp.com). D-(+)-glucose, ascorbic acid (AA), uric acid (UA) and glutaraldehyde were bought from Adamas Reagent Co. Ltd. (Shanghai, China; www.adamas-beta.com). Nafion (5%, *w*/*w*) was bought from Alfa Aesar (Shanghai, China; www.alfa.com). Other chemicals, such as H_2O_2, $[Fe(CN)_6]^{3-/4-}$, NaOH, HNO_3, HCl and KCl were obtained from Guangfu Tech. Co. Ltd. (Tianjin, China; www.guangfu-chem.com). 0.1 M phosphate buffer (pH 6.0) was prepared using 0.1 M KH_2PO_4 and 0.1 M K_2HPO_4. 0.1 M H_2O_2 stock solution was prepared by dilution of 30% H_2O_2. 0.1 M glucose solution was freshly prepared and stored overnight before use. Both stock solutions were stored at 4 °C and diluted before use. All the other reagents were of analytical grade and the solutions were prepared with double distilled water.

Apparatus

All electrochemical measurements were carried out with a computer-controlled CHI 660E electrochemical workstation (ChenHua Instruments Co., Shanghai, China; www.chinstr.com). The classical three-electrode system consists of a prepared electrode, a Ag/AgCl electrode and a platinum wire as working, reference and counter electrode, respectively. Electrochemical impedance spectroscopy (EIS) experiments were conducted at a potential of 200 mV in the frequency range from 0.01 Hz to 100 KHz with a signal amplitude of 5 mV. A CTP-2000 K dielectric barrier discharge (DBD) reactor (SuMan Electronics Co. Ltd., Nanjing, China; www.atobo.com.cn) was used for nitrogen doping of graphite. Surface morphologies of GF and PB/NGF were characterized by scanning electron microscopy (SEM, Zeiss Supra 55VP; www.bruker.com). For comparison, glucose concentrations of serum samples were also determined by LH750 biochemical analyzer (Beckman Coulter. USA; www.beckmancoulter.cn) as a standard method. X-ray photoelectron spectroscopy (XPS) was operated using an Al Kα X-ray source (Escalab 250, Thermo Fisher Scientific, USA; www.thermofisher.com). Raman spectra were recorded on a Lab RAM HR Raman microscope (Horiba Jobin Yvon, France; www.

horiba.com) with a laser ex-citation wavelength of 488 nm. Energy dispersive spectrometry (EDS) was conducted with a Nova Nano FESEM 450 at 10 k V equipped with Energy Dispersive X-ray Spectroscopy (Bruker XFlash-SDD-5010, Germany; www.bruker.com).

Fabrication of NGFE

Graphite foam (GF) was prepared by chemical vapor deposition (CVD) method similar to the previous report [18] as elaborated described in Supporting Information. After nickel foam used as the template completely removed, GF was carefully washed by distilled water and dried under IR light for subsequent use. Nitrogen-doped GF (NGF) was prepared in a DBD plasma system, in which NH_3-N_2 as working gas and treatment time of 10 min were chosen. Specific doping conditions of NGF were elaborated in the Supporting Information file. The NGF was cut into small pieces (10 mm × 5 mm, 1 mm thick) and fixed onto a glass plate. NGF electrode (NGFE) was then connected to the electrochemical system by conductive silver paste.

Preparation of PB/NGFE

The NGFE was then submerged into solution (pH 2.0) containing 3.0 mM $K_3[Fe(CN)_6]$, 3.0 mM $FeCl_3$ and 0.1 M KCl. Electrodeposition of PB was made via electro-oxidation using a constant potential of 0.4 V for 80 s. After deposition, PB particles was electrochemically activated in the same supporting electrolyte by scanning in the range of −0.05 ~ 0.35 V at 40 mV s^{-1} until stable voltammogram was obtained. Subsequently, the electrode was heated at 100 °C for 1 h [19], and PB modified NGFE (PB/NGFE) was finally ready.

Fabrication of GOx/PB/NGFE

Immobilization of GOx onto the surface of PB/NGFE was done by cross-linking method [20]. GOx enzymatic solution was prepared by dissolving 10 mg GOx lyophilized powder into 500 μL phosphate buffer, and then 8 μL glutaraldehyde (25 vol.%) and 5 μL BSA (20 *w*% diluted in water) were added to 87 μL prepared enzyme solution. 15 μL above mixture was dropped onto PB/NGFE surface and the electrode was left in oven at 37.5 °C for 3 h. Subsequently, 20 μL Nafion (0.5 vol.% in ethanol) was dropped onto the enzyme modified electrode in order to prevent possible enzyme leakage and diminish external interference. Finally, the electrode was immersed in water for 30 min to remove the non-immobilized enzyme and the glucose biosensor based on GOx/PB/NGFE was obtained. All enzyme electrodes were kept at 4 °C when not in use.

Glucose detection by GOx/PB/NGFE in human serum

Fresh serum samples were collected from local hospital. Prior to use, the samples were centrifuged at 7000 rpm for 15 min and the supernatant was adopted for analysis. Glucose detection using GOx/PB/NGFE was carried out in triplicate by adding 0.1 mL sample to an electrochemical cell containing 10.0 mL phosphate buffer with 0.1 M KCl (0.1 M, pH 6.0) at −0.05 V applied potential under continuous stirring. All the experiments were carried out at room temperature.The study was approved by the ethical committee and all sample providers signed the informed consent.

Results and discussion

Choice of materials

As we know, detection of oxidases's side product, H_2O_2, is a popular way for enzyme-based biosensors to detect relevant biomolecules. PB is not only more accessible but more active and selective for H_2O_2 detection than the commonly used platinum [21]. Compared with 2D planar electrodes, 3D GF possesses much larger surface area and faster electron transport rate, which is beneficial to getting high sensitivity. As a commonly doped heteroatom, herein N is introduced to endow better electron mobility of 3D GF.

Morphology and constituent characterization of electrodes

As can be seen from SEM images in Fig. 1a, NGF owns a 3D porous and interconnected network, which helps transportation of electrolyte and analyte and fast electron transport. Its pore size is about 200~400 μm and strut width is around 50 μm (inset of Fig. 1a). The inside hollow space stems from the original template-Ni foam and the deposition of thin graphite. After PB modification, (Fig. 1b), dispersed PB particles can be seen on the surface of the GF skeleton, which are round and uniform nanoparticles (inset of Fig. 1b) with an average diameter 195 ± 26.2 nm calculated by Image J and around 100 particles were taken into account. EDS spectra in Fig. S1 show existence of Fe atoms after PB deposition, confirming that PB particles were successfully prepared.

In XPS spectrum of NGF (Fig. 1c, red curve), peaks appeared at about 400 and 283 eV, which correspond to N 1 s and C 1 s, respectively. XPS spectrum of GF (Fig. 1c, black curve), by contrast, only had C 1 s (282.5 eV) and O 1 s (528.6 eV) peaks. The N 1 s peak verified existence of N element in the NGF nanocomposites and the atomic percentage of N was calculated to be about 1.49%. The inset of Fig. 1e displays high-resolution spectra of N 1 s,

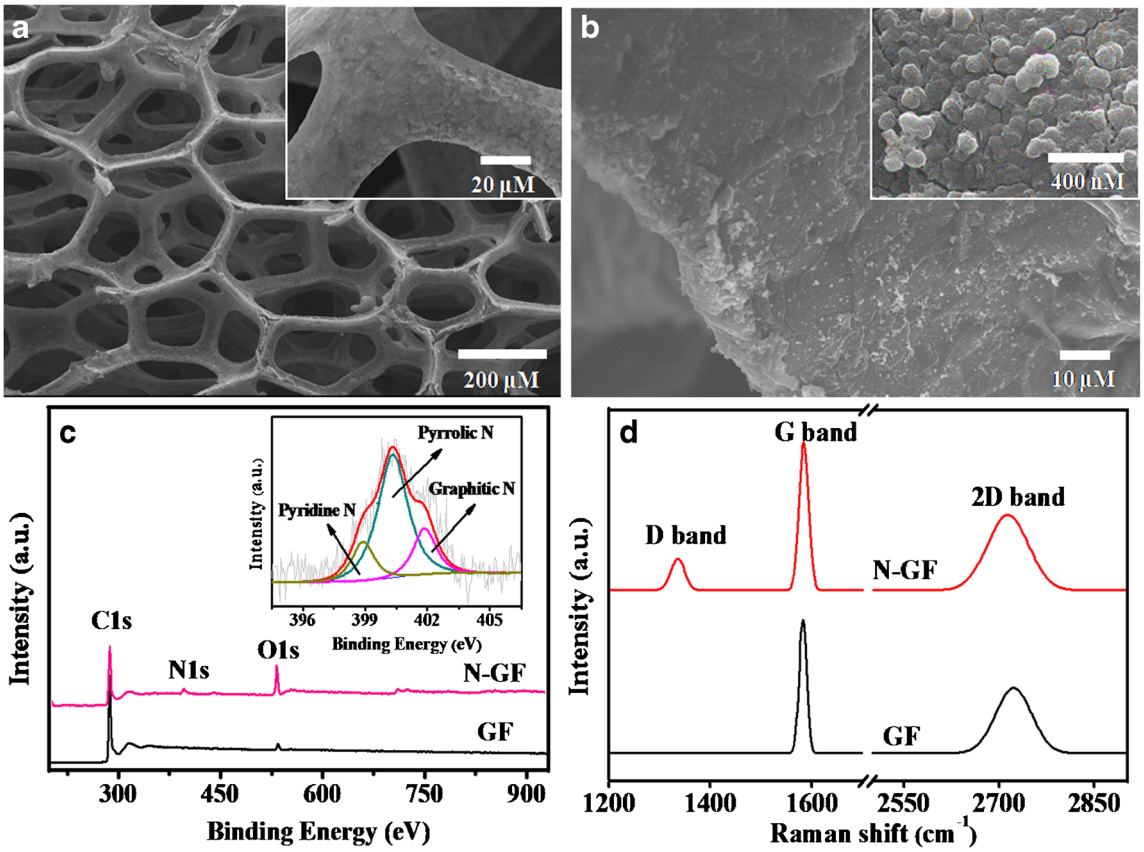

Fig. 1 SEM images of NGF (**a**) and PB decorated NGF (**b**). XPS spectra (**c**) and Raman spectra (**d**) of GF and NGF. Inset of (**a**) is the skeleton of NGF at higher magnification. Inset of (**b**) is PB particles deposited on NGF at higher magnification. Inset of (**c**) is zoom-in view of XPS spectra of N 1 s

which present three types of N, including pyridinic N (398.9 eV), pyrrolic N (400.3 eV) and graphitic N (401.9 eV). Fig. 2a displays the cyclic voltammograms (CV) scans of differently modified electrodes. Curve a and b showed no obvious redox peak in electrolyte solution. In contrast, after PB layer was deposited on NGF, a pair of well-defined peaks can be observed (curve c), which arise from PB redox reactions at electrode. When GOx was immobilized on PB/NGF surface, redox peak separation (ΔEp) increased (curve d). This may be ascribed to non-conductivity of GOx, slowing down electron transmission rate. CV scans of GF and NGF electrodes in 5.0 mM $Fe(CN)6^{3-/4-}$ are illustrated in Fig. 2c. Apparently, the redox peak current of NGF was significantly increased compared to GF. This is likely due to the N-doping into graphene, which increases the metallic behavior of GF and allows for easier electron transfer at electrode/electrolyte interface.

EIS was also used to monitor changes in interface property of different electrodes. The impedance spectra include semicircle portion at higher frequencies and linear portion at lower frequencies, which relates to the electron-transfer resistance and the diffusion process, respectively. As can be seen in Fig. 2b, EIS analysis displayed a reduced resistance for NGF (curve b) compared to GF (curve a). This was illustrated by semi-circular region in Nyquist plots in Fig. 2b. Electron-transfer resistance (R_{et}) was calculated by measuring the diameter of the high-frequency semicircle in the plots. At GF, small and well-defined semicircle was obtained with an interface impedance of 32.7 Ω. After N doping, the resistance of NGF was decreased to 11.6 Ω, originating from the excellent electron transport ability of NGF. As for PB/NGF (curve c), its resistance decreased compared to that of NGF, which can be attributed to the nanosized PB promoting electron transfer. When GOx was immobilized on PB/NGF, the resistance increased to 26.7 Ω (curve d), owing to poor conductivity of enzyme.

Fig. 2d shows the CV scans of PB/N-GF before and after addition of 2.0 mM H_2O_2. Curve a shows a pair of redox peaks at +0.115 V and +0.248 V, which corresponds to the PB/Prussan white (PW) redox transition. Specific redox reaction is shown in Eq. (1) [21]. After H_2O_2 addition, oxidation peak current of PW decreased, along with increased reduction peak current of PB (curve b), which arises from consumption of PW by reacting with H_2O_2, as shown in eq. (2). This

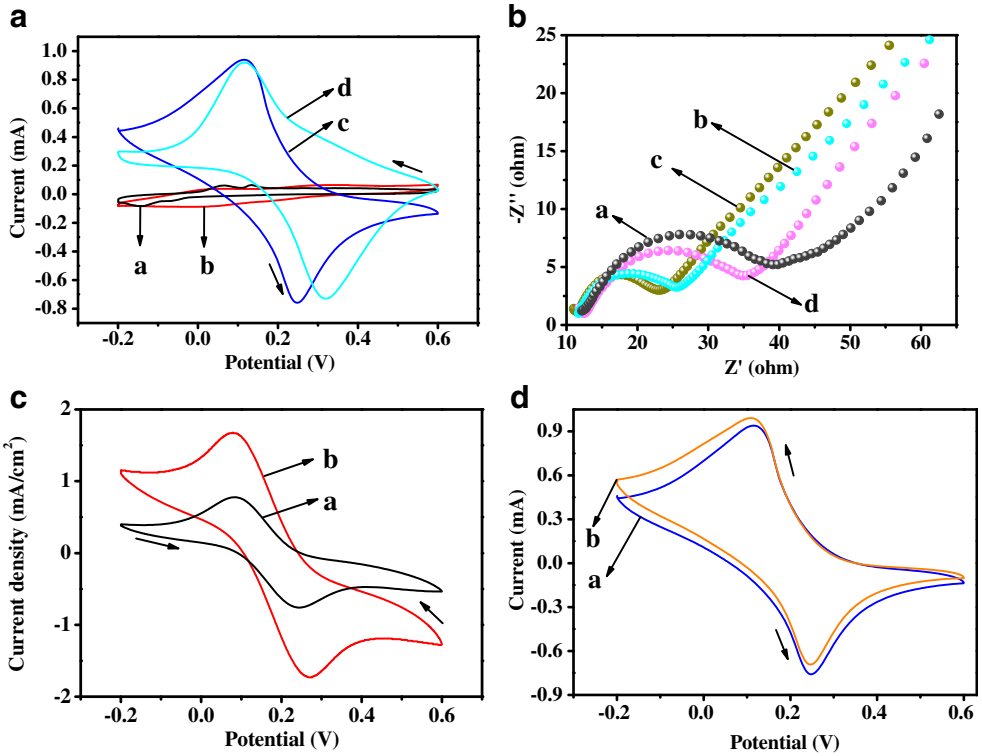

Fig. 2 CV scans (**a**) of GF (a), NGF (b), PB/NGF (c) and GOx/PB/NGF (d) in phosphate buffer containing 0.1 M KCl (pH 6.0). EIS Nyquist plots (**b**) of differently modified electrodes in 5.0 mM $Fe(CN)_6^{3-/4-}$ and 0.1 M KCl. CV scans (**c**) of GF (a) and NGF (b) in 5.0 mM $Fe(CN)_6^{3-/4-}$ and 0.1 M KCl. CV scans (**d**) of PB/N-GF in phosphate buffer before (a) and after (b) 2.0 mM H_2O_2 was added. Scan rate was 100 mV s^{-1}. Frequency range of EIS was 0.01 Hz~100 kHz

indicated high electrocatalytic ability of the PB/NGF towards reduction reaction of H_2O_2.

$$\underset{\text{PB}}{Fe_4[Fe(CN)_6]_3} + 4K^+ + 4e^- \rightleftharpoons \underset{\text{PW}}{K_4Fe_4[Fe(CN)_6]_3} \quad (1)$$

$$\underset{\text{PW}}{K_4Fe_4[Fe(CN)_6]_3} + 2H_2O_2 \rightleftharpoons \underset{\text{PB}}{Fe_4[Fe(CN)_6]_3} + 4K^+ + 4OH^- \quad (2)$$

Optimization of PB deposition time and PB stability

Electrochemical deposition time has influence on the number of PB particles deposited on NGFE [22], and thus effects the performance of PB modified NGFE. Different periods of time (40, 60, 80 and 100 s) for PB electrodeposition on NGF were investigated and the CV scans of the PB/NGF were compared. As can be observed in Fig. 3a, bare NGFE (0 s) gave no redox peak in phosphate buffer. With increase of the deposition time, peak current showed a substantial increase due to accumulation of PB particles. At deposition time of 100 s, peak potential shifted notably, implying slowed electron transfer rate, which may be caused by stacked PB crystals raising ohmic resistance [23]. Therefore, PB deposition time was fixed to 80 s as it provides adequate surface coverage of PB on electrode and ensures good conductivity.

Evaluation of PB stability was also performed via CV, where the peak currents of PB/NGFE were compared before and after 250 scanning cycles. 2.12% decrease of reduction peak current was observed after 250 cycles, indicating good stability of PB layer on NGF. This is not only because the potassium cations in electrolyte do not damage the structure of electrodeposited PB on electrode [24], but also because nanostructure of NGF is favorable for immobilizing PB [23].

Detection of H_2O_2 by PB/NGFE

Electrocatalytic activity of PB/NGFE towards H_2O_2 reduction was studied with amperometric i-t curve (Fig. 3b). Calibration curve for H_2O_2 determination was presented in Fig. 3c and a good linearity was obtained at the concentration range from 0.004 mM to 1.6 mM. The regression equation of the linear part of the curve was $I\,(\mu A) = 0.964C\,(\mu M) + 0.006$ with R^2 of 0.9992. Limit of detection (LOD) was 2.4 μM (at an S/N ratio of 3) and sensitivity was 386 mA M^{-1} cm^{-2}. The response time at 90% of the steady state was within 10 s.

Amperometric determination of glucose at GOx/PB/NGFE

Calibration curve and detection limit

GOx served as model enzyme in order to test enzyme immobilization ability of PB/NGF. Fig. S2 gives an overview on the involved reactions, in which GOx catalyzes oxidation of glucose and the produced H_2O_2 is then reduced by PW as described in Section 3.2. Fig. 4a shows the amperometric responses of GOx/PB/NGFE to glucose at different concentrations (0.1~32 mM). The response time at 90% of the steady

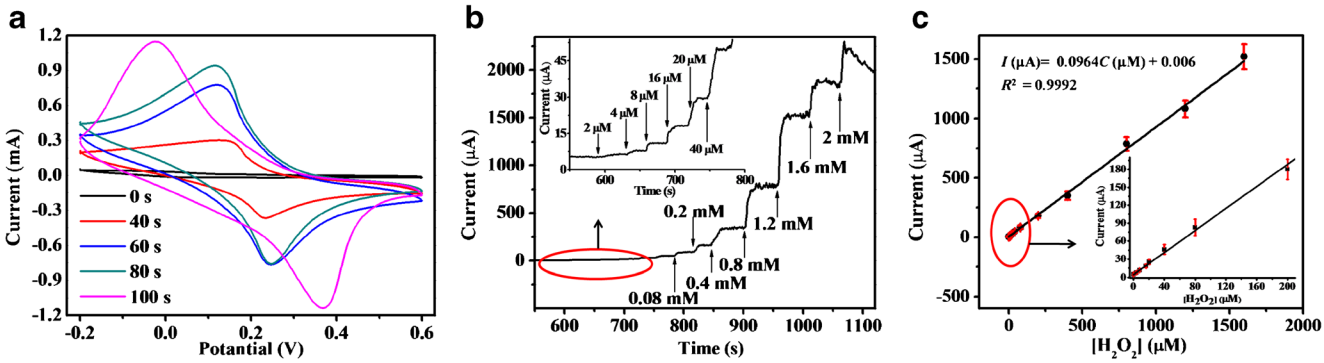

Fig. 3 CV scans (**a**) of NGF after electrodeposition of PB at 0, 20, 40, 60, 80, 100 s in phosphate buffer containing 0.1 M KCl (pH 6.0). Scan rate was 100 mV s^{-1}. Characteristic current-time plot (**b**) for PB/NGFE responses to successive additions of 0.002 to 4.0 mM of H_2O_2 in phosphate buffer containing 0.1 M KCl (pH 6.0) at an applied potential of −50 mV vs. Ag/AgCl. Calibration curves (**c**) of PB/NGFE towards H_2O_2 ($n = 5$)

states was less than 40 s. The resulting calibration curve (Fig. 4b) was in the range from 0.2 mM to 20 mM and the regression equation was I (μA) = 6.87C (mM) + 0.011 with R^2 of 0.998. LOD (at an S/N ratio of 3) and sensitivity were calculated to be 0.1 mM and 27.48 mA M^{-1} cm^{-2}, respectively. Comparison of glucose detection is made among various graphene based biosensors, and the results are presented in Table 1. It can be found that our presented GOx/PB/NGF features a relatively wide linear range and satisfactory sensitivity.

Selectivity of GOx/PB/NGFE

In real samples like blood and urine, some coexisting substances may also generate electrical signals which interfere detection. Amperometric response of GOx/PB/NGFE was examined in the presence of foreign substances including fructose, lactose, galactose, maltose, AA and UA. It can be seen from Fig. 4b that UA and AA did not pose obvious effect on glucose assay. Besides, with addition of mono-saccharides (fructose and galactose) and disaccharides (maltose and lactose), no current change was observed. In contrast, 0.2, 1.0 and 2.0 mM glucose yield apparent current responses. Negligible effects of the interferents illustrated high selectivity of GOx/PB/NGF, which may be ascribed to the fact that GOx shows specific recognition toward glucose. In addition, low working potential (−50 mV vs. Ag/AgCl) applied in our work also contributes to the good selectivity as it is expected to reduce the reaction possibility of interferences [25].

Reproducibility and stability of GOx/PB/NGFE

Reproducibility was investigated by assaying 1.0 mM glucose, with 10 sensors prepared in the same manner. A relative standard deviation (RSD) of 4.24% was obtained, indicating good reproducibility. As for repeatability, glucose was detected at three concentrations (0.5 mM, 1.5 mM, and 3.0 mM) for 5 times; RSD of 3.45%, 5.23% and 4.47% were obtained for the three concentrations, respectively, reflecting that the sensor possessed good repeatability.

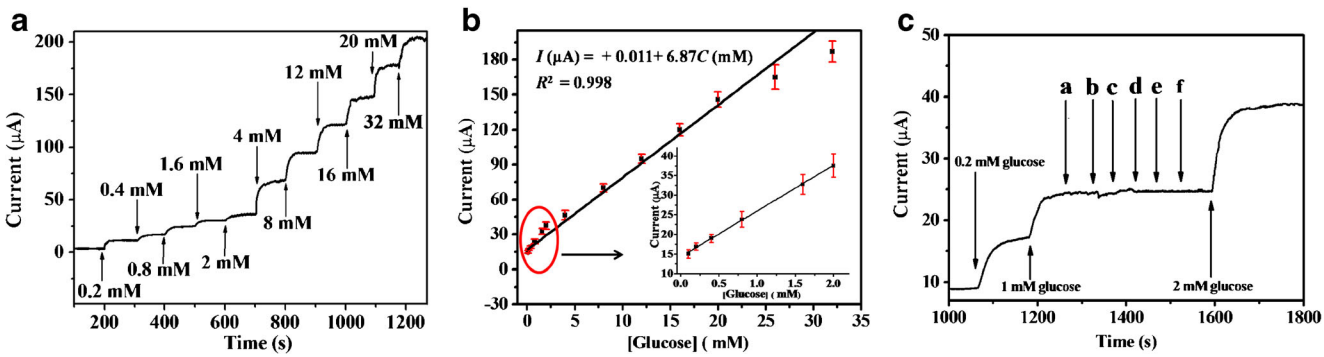

Fig. 4 Characteristic current-time plot (**a**) for GOx/PB/NGFE on successive step changes of glucose concentration from 0.1 mM to 32 mM in phosphate buffer containing 0.1 M KCl (pH 6.0) at an applied potential of −50 mV vs. Ag/AgCl. Corresponding calibration plot (**b**) of GOx/PB/NGFE towards glucose (n = 5). Amperometric response (C) towards UA (a), AA (b), fructose (c), galactose (d), maltose (e) and lactose (f) at GOx/PB/NGFE in phosphate buffer containing 0.1 M KCl (pH 6.0). The concentration of AA is 0.5 mM and that of the rest substances is 5.0 mM. The applied potential is −50 mV vs. Ag/AgCl

Table 1 Comparison of different graphene-based biosensors for determination of glucose

Electrode	Applied potential (V)	Linearity range (mM)	LOD (mM)	Sensitivity (mA M^{-1} cm^{-2})	References
$Ni(OH)_2$/[a]N-RGO/[b]GCE	0.45 vs. Ag/AgCl	0.5×10^{-3} ~11.5×10^{-3}	0.12×10^{-3}	3214	[26]
[b]GCE/[a]RGO/[c]pTB-[d]HRP-GOx	−0.1 vs. SCE	0.08 ~ 3.0	0.05	n.m.	[27]
[e]Cs/GOx/[f]ER[a]GO/[b]GCE	−0.45 vs. SCE	0.02~3.2	1.7×10^{-3}	6.82	[28]
[a]G/[g]AuNPs/GOx/[e]Cs/[h]GE	−0.2 vs. Ag/AgCl	2.0 ~ 10.0	0.18	0.55	[29]
[a]GO/PB/GOx/[e]Cs/[b]GCE	0.1 vs. SCE	0.1 ~ 13.5	3.4×10^{-4}	15.28	[30]
[i]ER-GNO/[j]IL-SPE	−0.20 vs. Ag/AgCl	0.005 ~ 10.0	0.001	22.8	[31]
[a]RGO/[k]AgNPs/[b]GCE	−0.25 vs. Ag/AgCl	0.032 ~ 1.89	4.5×10^{-3}	0.076	[32]
Fe_3O_4/[l]CG-GOx	0.5 vs. Ag/AgCl	0 ~ 26.0	0.016	5.66	[33]
3D GOx/PB/NGFE	−0.05 vs. Ag/AgCl	0.2 ~ 20.0	0.1	27.5	This work

[a] N-RGO: nitrogen-doped reduced graphene oxide; [b] GCE, glass carbon electrode; [c] pTB: poly (toluidine blue); [d] HRP: horseradish peroxidase; [e] CS, chitosan; [g] AuNPs, Au nanoparticle; [h] GE, gold electrode; [i] ER: electrochemically reduced graphene oxide; [j] IL-SPE: ionic liquid screen printing electrode; [k] AgNPs, Ag nanoparticle; [l] CG: chitosan-functionalized graphene; n.m.: data not mentioned

Long-term stability, which depends on both stability of PB particles and activity maintenance of GOx, is also an important factor for practical application. To ensure stability, the prepared biosensors were stored dry in a refrigerator (4 °C) when not in use. It was found that the sensing response to 1.0 mM glucose decreased by only 5.17% compared with the initial response after 30 days, demonstrating good stability of GOx/PB/NGFE.

Real sample test

Glucose in human serum was analyzed by using the presented sensor. For the purpose of comparing and evaluating the performance of our method, commercial biochemical analyzer was employed in parallel to test serum samples. As shown in Table 2, the measurement results of GOx/PB/NGFE coincided with those of the biochemical analyzer, and the recovery was in the range of 89~101%. A *t*-test was performed at the 95% confidence interval and showed no significant difference in the detection data between the commercial analyzer and GOx/PB/NGFE, indicating high reliability of our method.

Conclusion

A novel PB/NGF sensing platform was fabricated, in which N-doping via DBD plasma enhanced electrochemical performance of the platform and PB electrodeposition afforded accurate determination of H_2O_2. In addition, the platform exhibits other advantages: i) multiple conductive networks of NGF allow for fast electron transport; ii) mechanical strength of NGF makes it a self-supporting electrode. After GOx was integrated on PB/NGF, the biosensor system has been successfully applied for determination of glucose in human serum. The 3D PB/NGF platform is not limited to GOx loading, but expected to serve as an effective supporter for a wide range of enzymes and other biological substances as well, which holds great promise for biosensing applications. It should be noted that one disadvantage related is electrode fouling from 3D macroporous structure of GF, which may be a hinder for glucose determination in vivo. Future work will be focused on alleviation of fouling, possibly via doping or modification on GF surface.

Table 2 Determination of glucose in human blood serum samples ($n = 3$)

Serum samples	Found by Biochemical Analyzer (mM)[a]	Added (mM)	Found by sensor (mM)[a]	Recovery (%)
1	4.77 ± 0.07	0	4.93 ± 0.20	–
	5.10 ± 0. 010	0.30	5.04 ± 0.31	90.1
	5.32 ± 0.20	0.60	5.33 ± 0.26	93.3
2	5.52 ± 0.09	0	5.60 ± 0.14	–
	5.81 ± 0.12	0.30	5.82 ± 0.29	99.8
	6.11 ± 0.03	0.60	6.13 ± 0.23	101.2
3	6.31 ± 0.11	0	6.39 ± 0.09	–
	6.67 ± 0.08	0.30	6.58 ± 0.27	89.3
	7.17 ± 0.12	0.60	6.87 ± 0.23	93.8

[a] The data were shown as (mean ± S.D.) for three separate measurements, where S.D. stands for standard deviation

Acknowledgments The project financially supported by National Natural Science Foundation of China (81773680, 81460543).

Compliance with ethical standards The author(s) declare that they have no competing interests.

References

1. Benvidi A, Tezerjani MD, Moshtaghiun SM, Mazloum-Ardakani M (2016) An aptasensor for tetracycline using a glassy carbon modified with nanosheets of graphene oxide. Microchim Acta 183(5):1797–1804
2. Li Y, Song H, Zhang L, Zuo P, Ye BC, Yao J, Chen W (2016) Supportless electrochemical sensor based on molecularly imprinted polymer modified nanoporous microrod for determination of dopamine at trace level. Biosens Bioelectron 78:308–314
3. Wang L, Li J, Pan Y, Min L, Zhang Y, Hu X, Yang Z (2017) Platinum nanoparticle-assembled nanoflake-like tin disulfide for enzyme-based amperometric sensing of glucose. Microchim Acta 184(7):2357–2363
4. Babacan S, Pivarnik P, Letcher S, Rand AG (2000) Evaluation of antibody immobilization methods for piezoelectric biosensor application. Biosens Bioelectron 15(11–12):615–621
5. Tuukkanen S, Virtanen J, Hytönen VP, Kulomaa MS, Törmä P (2003) Fabrication of DNA monolayers on gold substrates and guiding of DNA with electric field. Rev Adv Mater Sci 5(3):228–231
6. Ji J, Ji H, Zhang LL, Zhao X, Bai X, Fan X, Zhang F, Ruoff RS (2013) Graphene-encapsulated Si on ultrathin-graphite foam as anode for high capacity lithium-ion batteries. Adv Mater 25(33): 4673–4677
7. Yadav A, Kumar R, Bhatia G, Verma GL (2011) Development of mesophase pitch derived high thermal conductivity graphite foam using a template method. Carbon 49(11):3622–3630
8. Luong JHT, Glennon JD, Gedanken A, Vashist SK (2017) Achievement and assessment of direct electron transfer of glucose oxidase in electrochemical biosensing using carbon nanotubes, graphene, and their nanocomposites. Microchim Acta 184(2): 369–388
9. Li Y, Liu J, Liu M, Yu F, Zhang L, Tang H, Ye BC, Lai L (2016) Fabrication of ultra-sensitive and selective dopamine electrochemical sensor based on molecularly imprinted polymer modified graphene@carbon nanotube foam. Electrochem Commun 64:42–45
10. Xi F, Zhao D, Wang X, Chen P (2013) Non-enzymatic detection of hydrogen peroxide using a functionalized three-dimensional graphene electrode. Electrochem Commun 26(1):81–84
11. Jeong HM, Lee JW, Shin WH, Choi YJ, Shin HJ, Kang JK, Choi JW (2011) Nitrogen-doped graphene for high-performance ultracapacitors and the importance of nitrogen-doped sites at basal planes. Nano Lett 11(6):2472–2477
12. Liang J, Jiao Y, Jaroniec M, Qiao SZ (2012) Sulfur and nitrogen dual-doped mesoporous graphene electrocatalyst for oxygen reduction with synergistically enhanced performance. Angew Chem Int Ed Engl 51(46):11496–11500
13. Carrerosanchez JC, Elías AL, Mancilla R, Arrellín G, Terrones H, Laclette JP, Terrones M (2006) Biocompatibility and toxicological studies of carbon nanotubes doped with nitrogen. Nano Lett 6(8): 1609–1611
14. Gamero M, Pariente F, Lorenzo E, Alonso C (2010) Nanostructured rough gold electrodes for the development of lactate oxidase-based biosensors. Biosens Bioelectron 25(9):2038–2044
15. Chen X, Wu G, Cai Z, Oyama M, Xi C (2014) Advances in enzyme-free electrochemical sensors for hydrogen peroxide, glucose, and uric acid. Microchim Acta 181(7–8):689–705
16. Karpova EV, Karyakina EE, Karyakin AA (2017) Communication—accessing stability of oxidase-based biosensors via stabilizing the advanced H 2 O 2 transducer. J Electrochem Soc 164(5):B3056–B3058
17. Lin Y, Hu L, Yin L, Guo L (2015) Electrochemical glucose biosensor with improved performance based on the use of glucose oxidase and Prussian blue incorporated into a thin film of self-polymerized dopamine. Sensors Actuators B Chem 210:513–518
18. Ji H, Zhang L, Pettes MT, Li H, Chen S, Shi L, Piner R, Ruoff RS (2012) Ultrathin graphite foam: a three-dimensional conductive network for battery electrodes. Nano Lett 12(5):2446–2451
19. Ricci F, Amine A, Palleschi G, Moscone D (2003) Prussian blue based screen printed biosensors with improved characteristics of long-term lifetime and pH stability. Biosens Bioelectron 18(2–3):165–174
20. Ricci F, Amine A, Tuta CS, Ciucu AA, Lucarelli F, Palleschi G, Moscone D (2003) Prussian blue and enzyme bulk-modified screen-printed electrodes for hydrogen peroxide and glucose determination with improved storage and operational stability. Anal Chim Acta 485(1):111–120
21. Karyakin AA (2015) Prussian blue and its analogues: electrochemistry and analytical applications. Electroanalysis 13(10):813–819
22. Zhang X, Wang J, Ogorevc B, Spichiger UE (2015) Glucose Nanosensor based on Prussian-blue modified carbon-fiber cone Nanoelectrode and an integrated reference electrode. Electroanalysis 11(13):945–949
23. Yang P, Peng J, Chu Z, Jiang D, Jin W (2016) Facile synthesis of Prussian blue nanocubes/silver nanowires network as a water-based ink for the direct screen-printed flexible biosensor chips. Biosens Bioelectron 92:709–717
24. Nossol E, Zarbin AJG (2009) A simple and innovative route to prepare a novel carbon nanotube/Prussian blue electrode and its utilization as a highly sensitive H2O2 Amperometric sensor. Adv Funct Mater 19(24):3980–3986
25. Karyakin AA, Karyakina EE (1999) Prussian blue-based 'artificial peroxidase' as a transducer for hydrogen peroxide detection. Application to biosensors. Sensors Actuators B Chem 57(1–3):268–273
26. Zhang Y, Lei W, Wu Q, Xia X, Hao Q (2017) Amperometric nonenzymatic determination of glucose via a glassy carbon electrode modified with nickel hydroxide and N-doped reduced graphene oxide. Microchim Acta 184(9):3103–3111
27. Wang F, Gong W, Wang L, Chen Z (2015) Enhanced amperometric response of a glucose oxidase and horseradish peroxidase based bienzyme glucose biosensor modified with a film of polymerized toluidine blue containing reduced graphene oxide. Microchim Acta 182(11–12):1949–1956
28. Cui M, Xu B, Hu C, Shao HB, Qu L (2013) Direct electrochemistry and electrocatalysis of glucose oxidase on three-dimensional interpenetrating, porous graphene modified electrode. Electrochim Acta 98(16):48–53
29. Shan C, Yang H, Han D, Zhang Q, Ivaska A, Niu L (2009) Graphene/AuNPs/chitosan nanocomposites film for glucose biosensing. Biosens bioelectron. Biosens Bioelectron 25(5):1070–1074
30. Yao Z, Sun X, Zhu L, Shen H, Jia N (2011) Electrochemical sensing based on graphene oxide/Prussian blue hybrid film modified electrode. Electrochim Acta 56(3):1239–1245
31. Ping J, Wang Y, Fan K, Wu J, Ying Y (2011) Direct electrochemical reduction of graphene oxide on ionic liquid doped screen-printed electrode and its electrochemical biosensing application. Biosens Bioelectron 28(1):204–209
32. Luo Z, Yuwen L, Han Y, Tian J, Zhu X, Weng L, Wang L (2012) Reduced graphene oxide/PAMAM–silver nanoparticles nanocomposite modified electrode for direct electrochemistry of glucose oxidase and glucose sensing. Biosens Bioelectron 36(1):179–185
33. Zhang W, Li X, Zou R, Wu H, Shi H, Yu S, Liu Y (2015) Multifunctional glucose biosensors from Fe_3O_4 nanoparticles modified chitosan/graphene nanocomposites. Sci Rep-UK 5:11129